J Nanostruct 16(4): 5891-5899, Autumn 2026

RESEARCH PAPER

Physicochemical Characterization and Preliminary Antibacterial Responses of Artemisia herba-alba–Mediated Gold Nanoparticle Preparations from Otitis Media Isolates

Sahira Abd Alhasan Helal *, Rahman Laibi Chelab

Biology Department, College of Education for Pure Science, Thi-Qar University, Thi-Qar, Iraq

ARTICLE INFO

Article History:
Received 24 June 2026
Accepted 19 September 2026
Published 01 October 2026

Keywords:
Antibacterial screening
Artemisia herba-alba
Biofilm-associated biomass
Green synthesis
Gold-containing nanoparticle preparation

ABSTRACT

This study investigated the green synthesis, physicochemical characteristics, and in vitro antibacterial activity of *Artemisia herba-alba*-mediated gold-containing nanoparticles against bacterial isolates associated with otitis media. Among 110 clinical specimens, 87 (79.1%) yielded bacterial growth, with *Pseudomonas aeruginosa* (49.4%) and *Staphylococcus aureus* (37.9%) being the predominant isolates. The ethanolic extraction of *A. herba-alba* yielded 40% crude extract, which was subsequently used for nanoparticle synthesis. UV–visible spectroscopy revealed an absorption feature at 278 nm and a weak visible-region band at approximately 581–587 nm. FTIR analysis indicated the presence of organic functional groups potentially involved in nanoparticle formation and stabilization. TEM revealed approximately spherical nanoscale structures measuring 24.90–34.92 nm, whereas SEM showed larger apparent dimensions of 63.15–83.73 nm. XRD analysis indicated crystalline features, with a reported crystallite size of 20.85 nm. Antibacterial screening demonstrated inhibition zones of 19 mm against *S. aureus* and 23 mm against *P. aeruginosa* at a nominal preparation concentration of 64 µg/mL. MIC and MBC values ranged from 32–128 µg/mL and 64–256 µg/mL, respectively, among the tested isolates. The crystal-violet assay yielded a post-treatment absorbance of 0.073 ± 0.009 at 630 nm, providing a descriptive measure of biofilm-associated biomass. Overall, the findings demonstrate the in vitro antibacterial potential of *A. herba-alba*-mediated gold-containing nanoparticle preparations and support further investigation of their antimicrobial properties against otitis media-associated bacterial pathogens.

How to cite this article
Abd Alhasan Helal S., Laibi Chelab R. Physicochemical Characterization and Preliminary Antibacterial Responses of Artemisia herba-alba–Mediated Gold Nanoparticle Preparations from Otitis Media Isolates. J Nanostruct, 2026; 16(4):5891-5899. DOI: 10.22052/JNS.2026.04.116

INTRODUCTION

Antimicrobial resistance is a major global health challenge that reduces the effectiveness of conventional antibacterial therapy [1]. Resistance can arise through intrinsic and acquired mechanisms and must be documented by susceptibility testing for the particular isolates studied. Several bacterial species, including Pseudomonas aeruginosa, *Staphylococcus aureus*, *Proteus mirabilis* and *Klebsiella pneumoniae*, may be recovered from patients with ear infections; their clinical significance depends on the infection subtype and sampling procedure.

* *Corresponding Author Email: sahrera.abd.helal@utq.edu.iq*

This work is licensed under the Creative Commons Attribution 4.0 International License.
To view a copy of this license, visit http://creativecommons.org/licenses/by/4.0/.

Biofilms are structured microbial communities embedded in an extracellular matrix. Biofilm-associated tolerance may complicate antimicrobial treatment, but reduced crystal-violet staining alone does not distinguish a specific antibiofilm mechanism from impaired bacterial growth [2, 3].

Bacterial efflux systems can decrease intracellular concentrations of antimicrobial compounds [4]. However, an ethidium bromide fluorescence phenotype alone does not demonstrate inhibition of a specific efflux pump.

Otitis media encompasses distinct clinical conditions, including acute otitis media, chronic suppurative otitis media and otitis media with effusion, with different sampling and microbiological considerations [5]. The subtype represented by the current clinical samples must be specified before broader comparisons are drawn. Nanomaterials are being explored as experimental antibacterial agents, but their performance depends on material composition, concentration and test conditions [6, 7].

Metallic nanoparticles have physicochemical properties that may facilitate interactions with bacterial cells. Proposed antimicrobial effects include changes in membrane integrity and permeability, interactions with cellular constituents, and oxidative stress; however, these mechanisms depend on nanoparticle composition, bacterial species and assay conditions and were not directly examined in the present study [8, 9].

Plant-mediated gold nanoparticle synthesis can involve phytochemical reduction of metal ions and stabilization of the resulting particles. Biological extracts may reduce reliance on added chemical reducing and capping agents, although the environmental impact and purity of any particular formulation should not be presumed without measurements [10, 11].

Artemisia herba-alba (Asteraceae) contains diverse secondary metabolites, including phenolic constituents and terpenoids. Such compounds may contribute to metal-ion reduction and surface stabilization during plant-mediated synthesis; however, the compounds responsible in the present preparation were not individually identified [12].

This study aimed to synthesize and characterize gold nanoparticles using *Artemisia herba-alba* extract and evaluate their in vitro antibacterial activity against bacterial isolates associated with otitis media, with particular emphasis on their effects on biofilm-associated biomass and bacterial responses to ethidium bromide.

MATERIALS AND METHODS

Sample collection

A total of 110 clinical swab specimens were collected from patients attending Al-Haboubi General Hospital and Al-Rifai General Hospital between 17 December 2025 and 30 March 2026. The reported sampling procedure included cleaning the external ear with 70% ethanol before collection.

Clinical diagnoses were made by specialist physicians, and patient information was collected using dedicated forms. The study was approved by the Thi Qar Health Department (approval No. 44852, dated 17 December 2025).

Samples were collected and sent to the laboratory of the College of Education for Pure Sciences, Thi Qar University, to culture bacteria and identify species. Cultures were grown on nutrient agar, blood agar, MacConkey agar and chocolate agar and incubated aerobically at 37°C for 18–24 hours.

Artemisia herba-alba plant material was collected from the natural environment in Iraq and identified by Dr. Yas Khudair Abbas, a retired specialist in plant taxonomy formerly affiliated with the College of Education for Pure Sciences, University of Thi-Qar. The plant material was transferred to the laboratory for preparation of the ethanolic extract.

Identification of bacterial isolates

Identification of bacterial isolates was done on the basis of morphological, microscopic, and biochemical characteristics. The identification was later confirmed by the VITEK 2 Compact system.

Preparation of Artemisia herba-alba ethanolic extract

Leaves of *Artemisia herba-alba* were washed with distilled water, dried and powdered. A total of 40 g of dried plant powder was extracted in four separate batches, each comprising 10 g of powder and 50 mL of 95% ethanol (200 mL ethanol in total). Each batch was held at 37 °C for 24 h and filtered, and solvent was removed by rotary evaporation at 40 °C. The reported pooled mass of dried crude extract was 16 g, corresponding to a crude extraction yield of 40% by mass. The extract was stored at 4 °C until use [13].

CC BY

Extraction yield (%) = (Mass of dried extract / Mass of dried plant material) × 100

The reported crude extraction yield was (16 g / 40 g) × 100 = 40%. The 16 g refers to total crude dry material recovered from four batches, not the yield of an individual 10 g extraction.

Preparation of $HAuCl_4$ solution

A 1 mM solution of gold chloride ($HAuCl_4$) was prepared using double-distilled deionized water for green synthesis of AuNPs.

Green synthesis of AuNPs

A stock solution was prepared by dissolving 2 g of dried ethanolic extract in deionized distilled water to a nominal final volume of 10 mL (200 mg/mL). For synthesis, 10 mL of the extract solution was combined with 90 mL of 1 mM $HAuCl_4$ and stirred at room temperature for 30–60 min. The nominal crude-extract concentration in the reaction mixture was 20 mg/mL. A colour change from pale yellow to orange and dark red was observed. The product was centrifuged at 14,000 rpm for 20 min, washed three times with sterile distilled water, dried, resuspended and stored at 4 °C [14].

Characterization of AuNPs

The preparation was characterized by UV–visible spectroscopy across 190–1100 nm, FTIR spectroscopy over approximately 400–4000 cm^{-1}, transmission electron microscopy (TEM), scanning electron microscopy (SEM/FE-SEM) and X-ray diffraction (XRD). Spectroscopic measurements were used to examine optical absorption and functional groups, whereas microscopy and diffraction were used to assess morphology and crystalline features.

Antibacterial activity

Antibacterial activity was examined by agar-well diffusion on Mueller–Hinton agar using bacterial suspensions adjusted to 0.5 McFarland. Wells of 5 mm diameter were loaded with 50 µL of the preparation at a nominal concentration

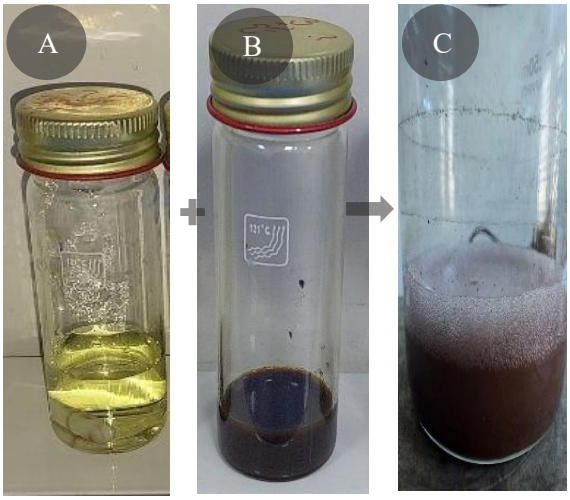

Fig. 1. Visual stages of the *A. herba-alba*-assisted synthesis: (A) $HAuCl_4$ solution, (B) plant extract, and (C) reaction mixture after synthesis.

Table 1. Reported VITEK 2 identification confidence for the listed bacterial species.

Isolate	Percentage
P. aeruginosa	97%
S. aureus	99%
P. mirabilis	99%
K. pneumoniae	99%

CC BY

of 64 µg/mL and incubated at 37 °C for 18–24 h. Distilled water was used as a vehicle control; crude plant extract and 1 mM $HAuCl_4$ were examined separately. Clindamycin (DA) and gentamicin (CN) were included as antibiotic comparators. Three wells were prepared per tested condition in the reported assay. Disk-diffusion zone measurements were tabulated for 33 *S. aureus* and 43 *P. aeruginosa* isolates.

Minimum inhibitory concentrations (MICs) were determined by serial broth dilution in Mueller–Hinton broth, with the lowest concentration showing no visible bacterial growth recorded as the MIC. Aliquots from growth-negative preparations were subcultured onto Mueller–Hinton agar and incubated for 18 h to obtain the reported minimum bactericidal concentration (MBC) endpoints.

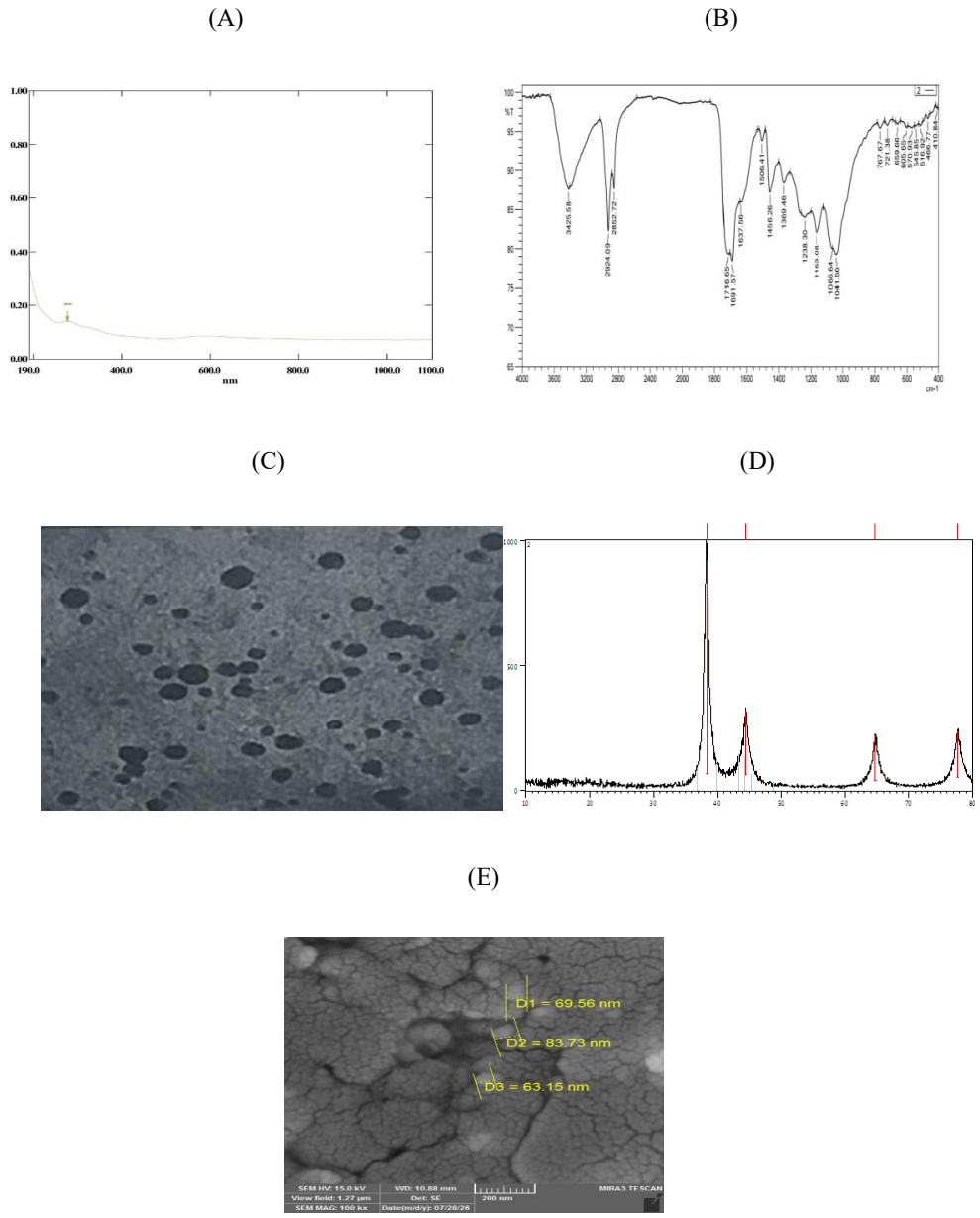

Fig. 2. Characterization of the preparation: (A) UV–visible absorption spectrum, (B) FTIR spectrum, (C) XRD diffraction pattern, (D) TEM micrograph and (E) FE-SEM micrograph.

Assessment of Biofilm Formation and Efflux Pump Activity

Biofilm-associated biomass was assessed using crystal-violet staining in microtiter plates, with absorbance measured at 630 nm after incubation for 24 h at 37 °C [27]. The reported treatment concentrations were 64 µg/mL for *P. aeruginosa* and 128 µg/mL for *S. aureus*. Untreated counterparts and three wells per condition were used.

The ethidium bromide cartwheel assay was carried out at dye concentrations of 0.5, 1, 1.5 and 2 µg/mL [28]. After incubation, fluorescence was assessed visually under UV illumination using an ordinal scale in which +2 indicated strong fluorescence.

RESULTS AND DISCUSSION

Bacterial isolation and identification

Among 110 clinical specimens, 87 (79.1%) were culture positive and 23 (20.9%) were culture negative. The distribution among positive specimens was *P. aeruginosa* (43; 49.4%), *S. aureus* (33; 37.9%), *P. mirabilis* (10; 11.5%) and *K. pneumoniae* (1; 1.1%). Isolates were identified by conventional microbiological examination and the VITEK 2 Compact system (Table 1). Table 1 reports representative identification-confidence values rather than resistance percentages.

Biosynthesis and characterization of AuNPs

The reaction mixture changed from pale yellow to orange/dark red during synthesis (Fig. 1). The UV–visible spectrum (190–1100 nm) exhibited an absorption feature at 278 nm (absorbance 0.141) and a weak broad visible-region feature near 581–587 nm (absorbance approximately 0.085; Fig. 2A). The ultraviolet feature may include contributions from plant-derived constituents, while the broad visible feature may be compatible with a plasmon-associated optical response.

The FTIR spectrum (Fig. 2B) contained a broad band at 3425.58 cm^{-1}, tentatively assigned to O–H stretching, and bands at 2924.09 and 2852.72 cm^{-1} associated with aliphatic C–H stretching. Bands at 1716.65 and 1691.57 cm^{-1} suggested carbonyl-related vibrations; the band at 1637.56 cm^{-1} may reflect C=C stretching or water bending. Bands at 1506.41, 1456.26 and 1369.46 cm^{-1} were tentatively attributed to aromatic skeletal vibrations and C–H bending. Features at 1238.30, 1163.08, 1066.64 and 1041.56 cm^{-1} were consistent with C–O and C–O–C vibrations. These functional groups are consistent with the presence of organic compounds associated with the preparation.

TEM images showed predominantly near-spherical structures with reported diameters of 24.90–34.92 nm, whereas SEM images showed larger apparent dimensions of 63.15–83.73 nm, potentially reflecting particle association (Fig. 2). XRD reflections were assigned to the (111), (200), (220) and (311) planes, with an estimated coherent crystallite size of 20.85 nm.

For XRD, coherent crystallite size is conventionally estimated using the Scherrer relation, $D = K\lambda/(\beta \cos \theta)$, where K is the shape factor, λ is the X-ray wavelength, β is the corrected peak full width at half maximum in radians and θ is the Bragg angle.

Antibacterial activity

At a nominal concentration of 64 µg/mL, the preparation produced inhibition zones of 19 mm against *S. aureus* and 23 mm against *P. aeruginosa*. Crude plant extract alone produced reported zones of approximately 6–10 mm, whereas the precursor solution (1 mM $HAuCl_4$) produced no clear measurable external inhibition zone in the observations supplied. Antibiotic disk-diffusion measurements for clindamycin (DA) and gentamicin (CN) were recorded for 33 *S. aureus* and 43 *P. aeruginosa* isolates and are summarized descriptively in Table 3.

The reported MIC and MBC values varied across the examined isolates (Table 2). For *P. aeruginosa* Ps6 and Ps15, MIC values were 32 and 64 µg/mL and MBC values were 64 and 128 µg/mL,

Table 2. Reported isolate-specific MIC and MBC values for the AuNP preparation.

Bacterial isolate	MIC (µg/mL)	MBC (µg/mL)
P. aeruginosa Ps6	32	64
P. aeruginosa Ps15	64	128
S. aureus St1	128	256
S. aureus St9	128	256

respectively. For *S. aureus* St1 and St9, MIC and MBC values were 128 and 256 µg/mL, respectively.

The antibiotic-zone worksheets comprised 33 *S. aureus* and 43 *P. aeruginosa* isolates. The measurements are summarized as inhibition-zone diameters in Table 3; clinical susceptibility categories were not assigned.

Assessment of Biofilm Formation and Efflux Pump Activity

The mean post-treatment biofilm-associated absorbance at 630 nm was 0.073 ± 0.009. This value represents crystal-violet staining in the treated conditions and is not itself a percentage reduction in biofilm biomass.

In the ethidium bromide cartwheel assay, strong fluorescence (+2) was observed at 1.5 and 2 µg/mL dye concentrations. This result indicates a fluorescence response under the assay conditions, without uniquely identifying the underlying membrane-transport mechanism.

The present study investigated the green synthesis and antibacterial properties of gold nanoparticle preparations mediated by *Artemisia herba-alba* extract against bacterial isolates associated with otitis media. The findings demonstrate the potential of plant-mediated nanomaterial synthesis for producing preparations with measurable antibacterial activity. The physicochemical observations and biological responses provide complementary insights into the characteristics and possible antimicrobial applications of the synthesized material.

The transformation of the reaction mixture from pale yellow to dark red following the addition of *A. herba-alba* extract to $HAuCl_4$ suggests the involvement of plant-derived constituents in the reduction of gold ions and the formation of nanoscale structures. This interpretation is consistent with the established role of phytochemicals in the green synthesis of metallic nanoparticles. Phenolic compounds and other oxygen-containing constituents may participate in metal-ion reduction and surface stabilization, potentially influencing particle morphology and dispersion. Similar phytochemical-mediated processes have been described in previous studies involving plant-derived gold nanoparticles [10, 11, 15–17].

UV–visible spectroscopic analysis revealed an absorption feature at 278 nm and a weak, broad visible-region band near 581–587 nm. The ultraviolet feature may reflect contributions from plant-derived organic constituents, whereas the visible-region absorption could be associated with the optical response of gold-containing nanostructures. The relatively broad and weak visible band may reflect differences in particle

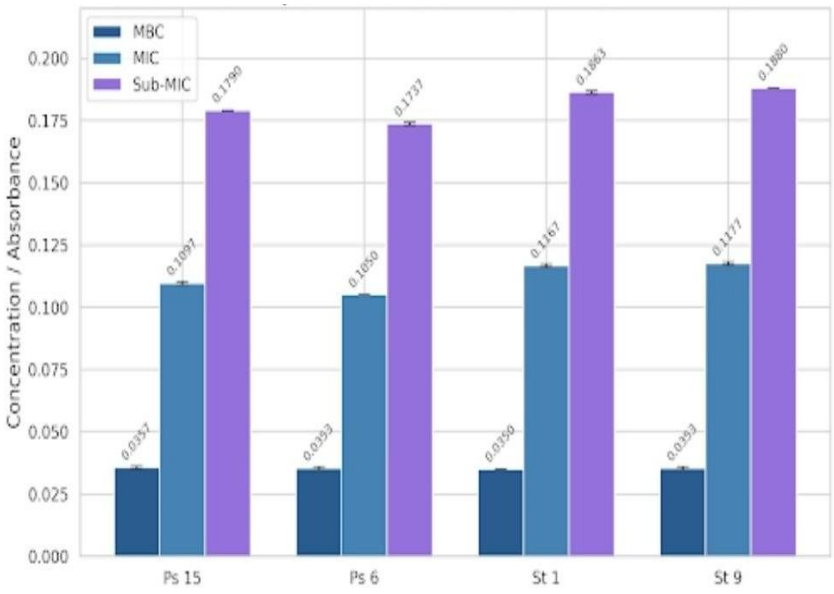

Fig. 3. Absorbance responses recorded under conditions designated MIC, MBC and sub-MIC for selected *P. aeruginosa* and *S. aureus* isolates.

CC BY

size, aggregation state, or interactions with the surrounding medium. These possibilities are relevant to the electron microscopy findings, which revealed differences between the particle dimensions observed by TEM and the larger apparent structures detected by SEM.

FTIR analysis provided additional information regarding the organic functional groups associated with the synthesized preparation. The broad absorption band at 3425.58 cm^{-1} suggests the presence of hydroxyl-containing constituents, while the bands at 1716.65 and 1691.57 cm^{-1} indicate carbonyl-related vibrations. Other absorption bands associated with C–H and C–O vibrations suggest the presence of additional organic components. These functional groups may contribute to the interaction between plant-derived molecules and the nanoparticle surface, thereby influencing particle stabilization.

The morphological and structural characterization revealed differences among the size estimates obtained using TEM, SEM, and XRD. TEM indicated predominantly spherical particles with diameters of approximately 24.90–34.92 nm, whereas SEM showed larger apparent dimensions ranging from 63.15 to 83.73 nm. These differences may be associated with particle aggregation, sample preparation, and the distinct imaging characteristics of the two techniques. XRD analysis indicated crystalline features assigned to the (111), (200), (220), and (311) planes, with a reported crystallite size of approximately 20.85 nm. The smaller XRD-derived value is not necessarily inconsistent with the TEM findings because crystallite size and particle diameter represent different structural characteristics. Together, these observations indicate nanoscale morphological and crystalline features, although detailed compositional and particle-size distribution analyses would further clarify the properties of the preparation.

The antibacterial screening demonstrated growth inhibition against both *Staphylococcus aureus* and *Pseudomonas aeruginosa*, with inhibition-zone diameters of 19 and 23 mm, respectively, at a reported concentration of 64 µg/mL. The larger inhibition zone observed for *P. aeruginosa* indicates a greater apparent response under the agar-diffusion conditions employed.

The observed antibacterial responses may involve interactions between nanoparticle-associated components and bacterial cell envelopes. Such interactions can influence membrane integrity and cellular functions, although the underlying mechanisms may vary between Gram-positive and Gram-negative organisms. *S. aureus* possesses a thick peptidoglycan layer, whereas *P. aeruginosa* has an outer membrane containing lipopolysaccharides that contributes to its permeability barrier. These structural differences may affect the interaction of the synthesized preparation with bacterial cells. Nevertheless, the present findings do not directly establish a specific membrane-disruption or oxidative-damage mechanism [22–24].

The MIC and MBC results provided additional information regarding isolate-dependent antibacterial responses. Among the tested *P. aeruginosa* isolates, Ps6 exhibited MIC and MBC values of 32 and 64 µg/mL, respectively, whereas Ps15 showed corresponding values of 64 and 128 µg/mL. In comparison, the *S. aureus* isolates St1 and St9 exhibited MIC and MBC values of 128 and 256 µg/mL, respectively. These findings indicate differences in the reported inhibitory endpoints among the tested isolates, with lower concentrations recorded for the two *P. aeruginosa* isolates. The reported MBC/MIC ratio was 2 for each isolate, a pattern consistent with closely related inhibitory and bactericidal endpoints under the assay conditions.

The inclusion of plant-extract and $HAuCl_4$ controls enabled a comparative assessment of the antibacterial activity of the synthesized AuNP preparation and its individual synthesis components. The lower inhibition responses reported for the plant extract and gold precursor suggest that the synthesized preparation exhibited

Table 3. Descriptive inhibition-zone measurements for clindamycin (DA) and gentamicin (CN) against the tested clinical isolates.

Species	Worksheet entries	Code	Zero readings	Nonzero range (mm)
S. aureus	33	DA	19	10–30
S. aureus	33	CN	12	10–28
P. aeruginosa	43	DA	38	14–30
P. aeruginosa	43	CN	21	10–30

CC BY

greater antibacterial activity under the tested conditions. Furthermore, the inhibition-zone measurements obtained using clindamycin and gentamicin revealed variations in antibiotic responses among the examined bacterial isolates, highlighting differences in their susceptibility patterns.

The crystal-violet assay yielded a post-treatment absorbance of 0.073 ± 0.009 at 630 nm, reflecting the amount of surface-associated biomass retained under the experimental conditions. Crystal-violet staining provides an estimate of total attached biomass, including bacterial cells and extracellular matrix components, without distinguishing between viable and nonviable cells. Accordingly, the observed absorbance may reflect changes in bacterial attachment, biofilm development, or overall bacterial growth. Such responses may also be influenced by growth inhibition at concentrations approaching the MIC, highlighting the importance of distinguishing general antibacterial effects from biofilm-specific activity [28, 29].

The ethidium bromide agar cartwheel assay demonstrated a concentration-dependent fluorescence response, with strong fluorescence (+2) observed at ethidium bromide concentrations of 1.5 and 2 µg/mL. This fluorescence pattern is consistent with intracellular accumulation of ethidium bromide when its uptake exceeds the bacterial capacity for extrusion. Since intracellular dye accumulation is influenced by both membrane permeability and active efflux mechanisms, the observed fluorescence provides a phenotypic indication of bacterial dye transport rather than direct evidence of efflux-pump inhibition. Accordingly, these findings contribute to the characterization of bacterial responses to ethidium bromide under the experimental conditions [30, 31].

Overall, the study demonstrates the feasibility of preparing *A. herba-alba*-mediated gold-containing nanoscale materials and identifies measurable antibacterial responses against selected otitis media-associated isolates. The integration of structural characterization with antibacterial screening provides a basis for further investigation of these preparations. Future work focusing on validated material composition, standardized antibacterial testing, quantitative biofilm measurements, and mechanism-specific assays would strengthen the interpretation of the observed biological activities and clarify their potential biomedical significance.

CONCLUSION

This study demonstrated the successful preparation of *Artemisia herba-alba*-mediated gold-containing nanomaterials with nanoscale morphological and crystalline characteristics. The synthesized preparation exhibited in vitro antibacterial activity against selected clinical isolates of *Staphylococcus aureus* and *Pseudomonas aeruginosa*, as demonstrated by inhibition-zone measurements and MIC/MBC assays. Furthermore, the crystal-violet and ethidium bromide assays provided additional insights into biofilm-associated responses and bacterial dye accumulation. Collectively, these findings highlight the potential of *A. herba-alba*-mediated nanomaterials as a promising platform for further antimicrobial research, particularly against bacterial pathogens associated with otitis media.

CONFLICT OF INTEREST

The authors declare that there is no conflict of interests regarding the publication of this manuscript.

REFERENCES

1. Chinemerem Nwobodo D, Ugwu MC, Oliseloke Anie C, Al-Ouqaili MTS, Chinedu Ikem J, Victor Chigozie U, et al. Antibiotic resistance: The challenges and some emerging strategies for tackling a global menace. J Clin Lab Anal. 2022;36(9).
2. Sionov RV, Steinberg D. Targeting the Holy Triangle of Quorum Sensing, Biofilm Formation, and Antibiotic Resistance in Pathogenic Bacteria. Microorganisms. 2022;10(6):1239.
3. Sindeldecker D, Stoodley P. The many antibiotic resistance and tolerance strategies of Pseudomonas aeruginosa. Biofilm. 2021;3:100056.
4. Akhavan Tafti F, Eslami G, Zandi H, Barzegar K. Mutations in nalc gene of Mex AB-OprM efflux pump in carbapenem resistant Pseudomonas aeruginosa isolated from burn wounds in Yazd, Iran. Iranian Journal of Microbiology. 2020.
5. Jung SY, Kim D, Park DC, Lee EH, Choi Y-S, Ryu J, et al. Immunoglobulins and Transcription Factors in Otitis Media. Int J Mol Sci. 2021;22(6):3201.
6. Thapa RK, Diep DB, Tønnesen HH. Topical antimicrobial peptide formulations for wound healing: Current developments and future prospects. Acta Biomater. 2020;103:52-67.
7. Gurunathan S, Qasim M, Choi Y, Do JT, Park C, Hong K, et al. Antiviral Potential of Nanoparticles—Can Nanoparticles Fight Against Coronaviruses? Nanomaterials. 2020;10(9):1645.
8. Mobed A, Hasanzadeh M, Seidi F. Anti-bacterial activity of gold nanocomposites as a new nanomaterial weapon to

CC BY

combat photogenic agents: recent advances and challenges. RSC Advances. 2021;11(55):34688-34698.
9. Yougbare S, Chang T-K, Tan S-H, Kuo J-C, Hsu P-H, Su C-Y, et al. Antimicrobial Gold Nanoclusters: Recent Developments and Future Perspectives. Int J Mol Sci. 2019;20(12):2924.
10. Zuhrotun A, Oktaviani DJ, Hasanah AN. Biosynthesis of Gold and Silver Nanoparticles Using Phytochemical Compounds. Molecules. 2023;28(7):3240.
11. Santhosh PB, Genova J, Chamati H. Green Synthesis of Gold Nanoparticles: An Eco-Friendly Approach. Chemistry (Easton). 2022;4(2):345-369.
12. Alshammari AF, Ouni S, Bouzidi M, Alshammari AS, Alzahrani EA, Alismail H, et al. Green synthesis and enhanced photocatalytic activity of ZnSe nanoparticles capped with Artemisia herba-alba and calligonum plants extracts. Sci Rep. 2026;16(1).
13. Abdallah BM, Ali EM. Therapeutic Potential of Green Synthesized Gold Nanoparticles Using Extract of Leptadenia hastata against Invasive Pulmonary Aspergillosis. Journal of Fungi. 2022;8(5):442.
14. Mittal AK, Chisti Y, Banerjee UC. Synthesis of metallic nanoparticles using plant extracts. Biotechnol Adv. 2013;31(2):346-356.
15. Mohammed AN, Obaid AK, Al-Salam HAA. Immunophysiological comparison for induced hepatocellular carcinoma treated by alcoholic extract and nano-extract of opuntia ficus indica. International Journal of Environmental Sciences. 2025;11(1s):744-754.
16. Latif ZAA, Mohammed AM, Abbass NM. Synthesis and characterization of polymer nanocomposites from methyl acrylate and metal chloride and their application. Polym Bull. 2019;77(11):5879-5898.
17. Jafarizad A, Safaee K, Gharibian S, Omidi Y, Ekinci D. Biosynthesis and In-vitro Study of Gold Nanoparticles Using Mentha and Pelargonium Extracts. Procedia Materials Science. 2015;11:224-230.
18. KeskİN C, Atalar MN, Baran Mf, Baran A. Environmentally Friendly Rapid Synthesis of Gold Nanoparticles from Artemisia absinthium Plant Extract and Application of Antimicrobial Activities. Iğdır Üniversitesi Fen Bilimleri Enstitüsü Dergisi. 2021;11(1):365-375.
19. Dyusebaeva MA, Berillo DA, Berganayeva AE, Berganayeva GE, Ibragimova NA, Jumabayeva SM, et al. Antimicrobial Activity of Silver Nanoparticles Stabilized by Liposoluble Extract of Artemisia terrae-albae. Processes. 2023;11(10):3041.
20. Aziz WJ, Abid MA, Hussein EH. Biosynthesis of CuO nanoparticles and synergistic antibacterial activity using mint leaf extract. Materials Technology. 2019;35(8):447-451.
21. Khan SU, Anjum SI, Ansari MJ, Khan MHU, Kamal S, Rahman K, et al. Antimicrobial potentials of medicinal plant's extract and their derived silver nanoparticles: A focus on honey bee pathogen. Saudi J Biol Sci. 2019;26(7):1815-1834.
22. Dykman L, Khlebtsov N. Gold nanoparticles in biomedical applications: recent advances and perspectives. Chem Soc Rev. 2012;41(6):2256-2282.
23. Lemire JA, Harrison JJ, Turner RJ. Antimicrobial activity of metals: mechanisms, molecular targets and applications. Nature Reviews Microbiology. 2013;11(6):371-384.
24. Silhavy TJ, Kahne D, Walker S. The Bacterial Cell Envelope. Cold Spring Harb Perspect Biol. 2010;2(5):a000414-a000414.
25. Andersson DI, Hughes D. Microbiological effects of sublethal levels of antibiotics. Nature Reviews Microbiology. 2014;12(7):465-478.
26. Kaplan JB. Antibiotic-Induced Biofilm Formation. The International Journal of Artificial Organs. 2011;34(9):737-751.
27. Stepanović S, Vuković D, Dakić I, Savić B, Švabić-Vlahović M. A modified microtiter-plate test for quantification of staphylococcal biofilm formation. J Microbiol Methods. 2000;40(2):175-179.
28. Martins M, McCusker MP, Viveiros M, Couto I, Fanning S, Pagès J-M, et al. A Simple Method for Assessment of MDR Bacteria for Over-Expressed Efflux Pumps. The Open Microbiology Journal. 2013;7(1):72-82.
29. Elgamoudi B, Korolik V. A Guideline for Assessment and Characterization of Bacterial Biofilm Formation in the Presence of Inhibitory Compounds. BIO-PROTOCOL. 2023;13(21).
30. Magana M, Sereti C, Ioannidis A, Mitchell CA, Ball AR, Magiorkinis E, et al. Options and Limitations in Clinical Investigation of Bacterial Biofilms. Clin Microbiol Rev. 2018;31(3).
31. Blair JMA, Piddock LJV. How to Measure Export via Bacterial Multidrug Resistance Efflux Pumps. mBio. 2016;7(4).

CC BY